Acta Biochim Biophys Sin, 2015, 47(3), 156–163
doi: 10.1093/abbs/gmu130
Advance Access Publication Date: 28 January 2015
Original Article

Original Article

Abnormal expression of vesicular transport proteins in pulmonary arterial hypertension in monocrotaline-treated rats

Hongliang Zhang, Qin Luo, Zhihong Liu*, Yong Wang, and Zhihui Zhao

Center for Pulmonary Vascular Diseases, State Key Laboratory of Cardiovascular Disease, Fuwai Hospital, National Center for Cardiovascular Diseases, Chinese Academy of Medical Sciences and Peking Union Medical College, Beijing 100037, China

*Correspondence address. Tel/Fax: +86-10-88396589; E-mail: liuzhihongfw@hotmail.com

Received 28 September 2014; Accepted 12 November 2014

Abstract

Intracellular vesicular transport is shown to be dysfunctional in pulmonary arterial hypertension (PAH). However, the expression of intracellular vesicular transport proteins in PAH remains unclear. To elucidate the possible role of these proteins in the development of PAH, the changes in the expressions of *N*-ethyl-maleimide-sensitive factor (NSF), α-soluble NSF attachment protein (α-SNAP), synaptosome-associated membrane protein 23 (SNAP23), type 2 bone morphogenetic receptor (BMPR2), caveolin-1 (cav-1), and endothelial nitric oxide synthase (eNOS) were examined in lung tissues of monocrotaline (MCT)-treated rats by real-time polymerase chain reaction and western blot analysis. In addition, caspase-3, also examined by western blot analysis, was used as an indicator of apoptosis. Our data showed that during the development of PAH, the expressions of NSF, α-SNAP, and SNAP23 were significantly increased before pulmonary arterial pressure started to increase and then significantly decreased after PAH was established. The expressions of BMPR2 and eNOS were similar to those of NSF, α-SNAP, and SNAP23; however, the expression of cav-1 was down-regulated after MCT treatment. Caspase-3 expression was increased after exposure to MCT. In conclusion, the expressions of NSF, α-SNAP, and SNPA23 changed greatly during the onset of PAH, which was accompanied by abnormal expressions of BMPR2, cav-1, and eNOS, as well as an increase in apoptosis. Thus, changes in NSF, α-SNAP, and SNAP23 expressions appear to be mechanistically associated with the development of PAH in MCT-treated rats.

Key words: pulmonary arterial hypertension, monocrotaline, vesicular transport

Introduction

Pulmonary arterial hypertension (PAH) is a syndrome caused by restricted flow through the pulmonary arterial circulation, resulting in increased pulmonary vascular resistance, and ultimately right heart failure [1]. Before 2003, the term primary pulmonary hypertension was used to describe both idiopathic PAH and familial PAH. The pathology of PAH is characterized by abnormal expansions of endothelial cells, medial hypertrophy, and adventitial thickening of pulmonary arteries, all of which lead to reduced arterial lumen, cycles of thrombosis and recanalization, and eventually progressive right ventricular hypertrophy and cardiac failure [2–4]. Before targeted therapy (using endothelin antagonists, prostacyclin analogs, and phosphodiesterase inhibitors) was developed, the medical management of PAH was directed at vasodilatation and anticoagulation, and the median survival for primary pulmonary hypertension was only 2.8 years, and the 1-, 3-, and 5-year survival rates were 68%, 48%, and 34%, respectively [5]. Even with modern targeted therapy, the median survival for PAH (whether idiopathic or familial) is 7

© The Author 2015. Published by ABBS Editorial Office in association with Oxford University Press on behalf of the Institute of Biochemistry and Cell Biology, Shanghai Institutes for Biological Sciences, Chinese Academy of Sciences.

Downloaded from https://academic.oup.com/abbs/article/47/3/156/1754516 by guest on 05 April 2024

years, and 1-, 3-, 5-, and 7-year survival rates are 91%, 74%, 65%, and 59%, respectively [6].

Previous studies have shown that the hallmark plexiform lesions in PAH consist of enlarged endothelial cells, fibroblasts, and smooth muscle cell elements, which contain increased endoplasmic reticulum, Golgi stacks, vacuolation, and Weibel–Palade bodies [7–9]. These characteristics have also been seen in experimental PAH models [10–15]. Recent studies have revealed the trapping of various vesicle transport tethers, soluble *N*-ethyl-maleimide-sensitive factor attachment proteins (SNAPs), membrane proteins, which serve as SNAP receptors (SNAREs), the loss or reduction of cell surface proteins [e.g. caveolin-1 (cav-1), endothelial nitric oxide synthase (eNOS), and type 2 bone morphogenetic receptor (BMPR2)], and the aberrant sequestration of these proteins in the endoplasmic reticulum, Golgi apparatus, and cytoplasmic vesicles in PAH lesions. This resulted in reduced cell surface/caveolar production of nitric oxide (NO), hypo-*S*-nitrosylation of the transport mediator proteins, hyperactivation of STAT3 and concomitant defect in bone morphogenic protein (BMP)/Smad signaling, and imbalance between cellular proliferation and apoptosis [16–23]. These findings indicate that intracellular vesicular transport is dysfunctional in the arterial lesions in PAH. However, the expressions of proteins associated with intracellular vesicular transport in PAH are unknown. In this study, changes in the expressions of proteins associated with intracellular vesicular transport, e.g. *N*-ethyl-maleimide-sensitive factor (NSF), α-SNAP, and SNAP23 (here SNAP stands for synaptosome-associated membrane protein, belongs to SNAREs), were investigated in rats treated with monocrotaline (MCT) for 1–21 days. In addition, changes in the expressions of membrane proteins (BMPR2, cav-1, and eNOS) and in the level of apoptosis were also examined.

Materials and Methods

Animals

Seventy eight pathogen-free, 6–7 weeks old, male Sprague-Dawley rats (body weight, 160–180 g; Vital River Lab Animal Technology Co., Ltd, Beijing, China) were used in this study. All protocols and procedures were reviewed and approved by the Institutional Animal Use Committee of Fuwai Hospital and the Cardiovascular Institute, Chinese Academy of Medical Sciences and Peking Union Medical College, in accordance with the *Regulations for the Administration of Affairs Concerning Experimental Animals*, which has been approved by the State Council and promulgated by the State Science and Technology Commission of China. The investigation conformed with the *Guidelines for the Care and Use of Laboratory Animals* published by the National Academy Press (NIH Publication No. 85-23, revised 1985).

Treatment protocol

Rats were randomly assigned to six groups with 13 rats in each group. In each group, nine rats were given MCT solution (Sigma, St Louis, USA) and four rats were given the same volume of normal saline as controls. MCT was dissolved in distilled water, adjusted to pH 7.4 with 0.5 M HCl and injected intraperitoneally (60 mg/kg). Then, on days 1, 2, 3, 7, 14, and 21 after injection, one group was randomly selected for the subsequent experiments.

Hemodynamic studies and tissue preparation

Rats were anesthetized via an intraperitoneal injection of chloral hydrate (2.5 mg/kg), placed in the supine position, incubated and ventilated with room air at 60 breaths/min with a pressure-cycled rodent ventilator (Zhejiang Medical University Laboratory Apparatus Factory, Hangzhou, China). After a sternal incision was made, a percutaneous needle (27 gauge) connected to a transducer and flushed with heparinized saline was directly inserted into pulmonary artery to measure pulmonary artery pressure. The correct positioning of the needle in pulmonary artery was confirmed by pressure waves before pulmonary arterial pressure was recorded. After exsanguination, the lungs were perfused with heparinized saline through the needle; then, the right lung, right ventricle, and left ventricle plus septum were collected. The lungs were axially sectioned, rapidly frozen in liquid nitrogen, and then stored at −80°C until use in subsequent analysis and determination of total cellular RNA and tissue proteins. The right ventricle and left ventricle plus septum were weighed. The development of PAH was determined by the pulmonary arterial pressure and the weight ratio of the right ventricle to the left ventricle plus septum [RV/(LV + S)].

Real-time polymerase chain reaction analysis

The mRNA expressions of vesicular transport proteins (NSF, α-SNAP, and SNAP23) and plasma membrane proteins (BMPR2, cav-1, and eNOS) were evaluated by semiquantitative real-time polymerase chain reaction (PCR). Total RNA was isolated from rat lungs with the Z3100 SV Total RNA Isolation System (Promega, Madison, USA), and then the RNA sample was reverse transcribed with the A3500 Reverse Transcription System (Promega) in 20 μl, according to the manufacturer's instructions. The PCR was conducted at the linear phase of the exponential reaction for each gene. The cDNA was amplified using the QPK-201 SYBR® Green Realtime PCR Master Mix (Toyobo, Osaka, Japan) in 20 μl reaction mixture, according to the manufacturer's instructions by the following program: 1 cycle of 95°C for 60 s, 40 cycles of 95°C for 15 s, and 56°C for 60 s. Amplification of the target genes was conducted on a 7300 Real-Time PCR System (Applied Biosystems, Foster City, USA) and monitored every cycle by examining the amount of SYBR Green fluorescence generated.

Western blot analysis

The frozen lung tissues were homogenized in cooled RIPA protein extract solution (30 mM Tris, 150 mM NaCl, 1 mM benzylsulfonyl fluoride, 1 mM sodium orthovanadate, 1% Nonidet P-40, and 10% glycerol, pH 7.5) with 100 mM PMSF and then centrifuged at 12,000 *g* for 20 min at 4°C; the concentration of protein was quantified by using the bicinchoninic acid protein assays. Equal amounts of protein (50 μg/lane) were separated by electrophoresis (60 V for 2 h) through 12% sodium dodecyl sulfate polyacrylamide gel in a Tris/HCl buffer system and then transferred onto nitrocellulose membranes (Millipore, Billerica, USA). The membranes were blocked with 5% skim milk for 1 h at room temperature and then incubated at 4°C overnight with mouse monoclonal antibody against NSF (1:500; Abcam Inc., Massachusetts, USA) or α-SNAP (1:500; Santa Cruz, Santa Cruz, USA), polyclonal goat antibodies against SNAP23 (1:100; Santa Cruz), BMPR2 (1:100; BD Biosciences, New Jersey, USA), cav-1 (1:1000; LifeSpan BioSciences, Inc., Seattle, USA) or eNOS (1:100; BD Biosciences), and polyclonal mouse antibody against caspase-3 (1:500; all from Santa Cruz), respectively. Then, the membranes were washed with phosphate-buffered saline and probed with the corresponding horseradish peroxide-conjugated secondary antibodies (1:5000; Protein Tech, Chicago, USA). Specific bands of target proteins were visualized by chemiluminescence. Target signals were normalized to β-actin (1:2000; Protein Tech) and analyzed semiquantitatively with Quantity One System (Bio-Rad, Hercules, USA).

Downloaded from https://academic.oup.com/abbs/article/47/3/156/1754516 by guest on 05 April 2024

Statistical analysis

Data were presented as the mean ± SD. Comparisons between groups were made by Student's *t*-test. If the variances were not homogeneous, Satterthwaite separate variance estimation *t*-test was used. If data were not normally distributed, Mann–Whitney *U* nonparametric test was used. Differences among groups were tested by one-way ANOVA. Two-sided *P* values were used. $P < 0.05$ was considered of significant difference.

Results

Establishment of PAH by MCT injection

Prior to the treatment, the body mass of the rats did not differ among all the six groups (days 1–21) ($F = 2.33$, $P = 0.051$). In contrast, from day 2 after injection, the average body mass was significantly lower in MCT-treated rats than in control rats; thus, MCT treatment led to growth retardation (**Fig. 1**). In MCT-treated rats, the mean pulmonary arterial pressure progressively increased from day 7 to day 21: day 7, 14.83 ± 1.54 mmHg (MCT treated) vs. 12.13 ± 1.44 mmHg (control), $P = 0.013$; day 14, 18.56 ± 2.53 mmHg (MCT treated) vs. 13 ± 1.35 mmHg (control), $P = 0.002$; day 21, 22.57 ± 3.25 mmHg (MCT treated) vs. 13.38 ± 2.17 mmHg (control), $P = 0.001$ (**Fig. 2**). The ratio of RV/(LV + S) gradually increased with MCT treatment from day 14 onwards: day 14, 0.38 ± 0.09 (MCT treated) vs. 0.25 ± 0.06 (control), $P = 0.024$; day 21, 0.5 ± 0.09 (MCT treated) vs. 0.27 ± 0.02 (control), $P < 0.001$ (**Fig. 3**), which indicated that the increased pulmonary arterial pressure resulted in a compensatory hypertrophy of the right ventricle.

Effect of MCT on mRNA expressions of NSF, α-SNAP, SNAP23, BMPR2, cav-1, and eNOS

Semiquantitative real-time PCR was used to detect changes in mRNA expressions of NSF, α-SNAP, SNAP23, BMPR2, cav-1, and eNOS in rat lung tissues following MCT treatment. Housekeeping gene glyceraldehyde-3-phosphate dehydrogenase was used as an internal control. Results are shown in **Fig. 4**. In MCT-treated rats, the level of NSF mRNA expression increased from day 2 (1.5 folds greater than that in control rats; $P = 0.019$), was highest on day 7 (9.2 folds greater than that in control rats; $P < 0.001$), and then significantly decreased to a level that was barely detectable ($P < 0.01$) from day 14. Similarly, the level of α-SNAP mRNA expression in MCT-treated rats increased on day 1 (3 folds greater than that in control rats; $P = 0.004$) and day 2 (1.7 folds greater than that in control rats; $P = 0.019$), returned to control levels on day 3 ($P = 0.18$) and day 7 ($P = 0.09$), and then greatly decreased from day 14 onwards ($P < 0.05$). In the first 3 days after injection, the level of SNAP23 mRNA expression was 2 to 3 folds greater in MCT-treated rats than that in the control rats ($P < 0.01$), but then started to decrease from day

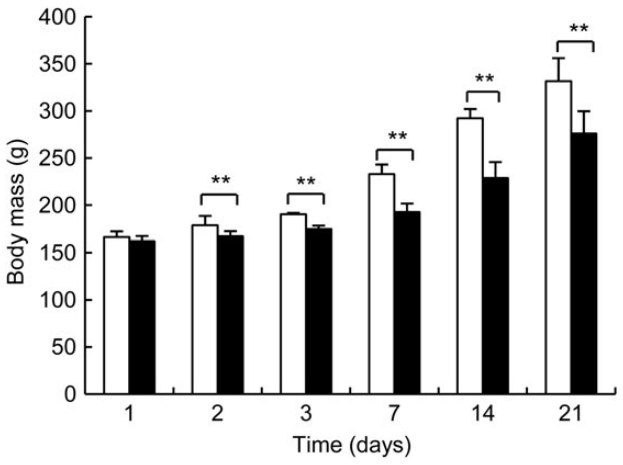

Figure 1. Effect of MCT on body mass Rats were sacrificed on days 1, 2, 3, 7, 14, and 21 after treatment with MCT. Rats treated with normal saline were used as controls. From day 2 onwards, average body mass was significantly lower in MCT-treated rats (solid bars; $n = 9$ for each bar) than in the control rats (open bars; $n = 4$ for each bar). $^{**}P < 0.01$ vs. control.

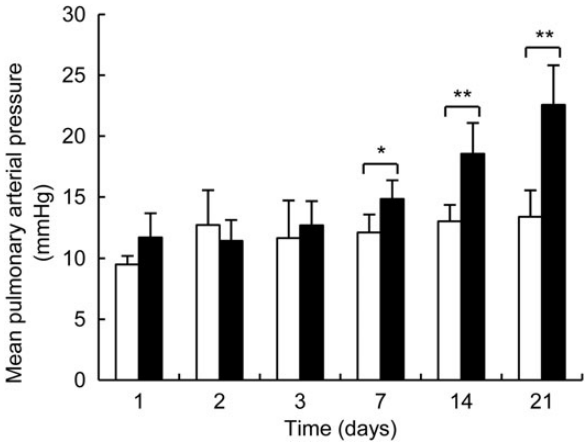

Figure 2. Effect of MCT on pulmonary arterial pressure The mean pulmonary arterial pressure of each rat was measured on days 1, 2, 3, 7, 14, and 21 after treatment with MCT or normal saline. The mean pulmonary arterial pressure progressively increased from day 7 to day 21. Open bars represent the data for the control rats ($n = 4$ for each bar), and solid bars represent the data for the MCT-treated rats ($n = 9$ for each bar). $^{*}P < 0.05$, $^{**}P < 0.01$ vs. control.

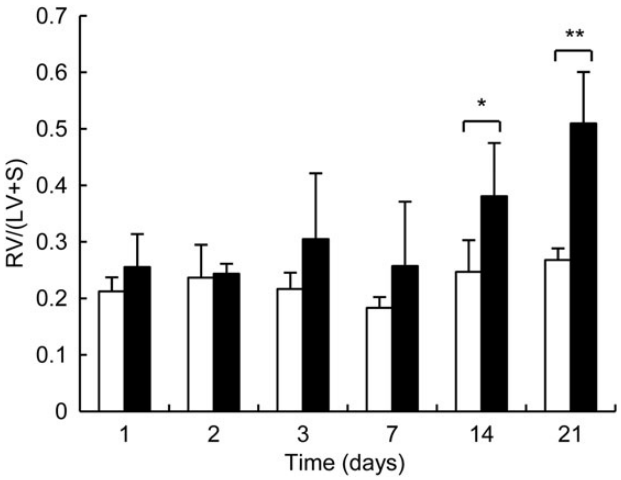

Figure 3. The effect of MCT on the ratio of the weight of the right ventricle to the combined weights of the left ventricle and the septum [RV/(LV + S)] The ratio of RV/(LV + S) was determined for each rat on days 1, 2, 3, 7, 14, and 21 after treatment with MCT or normal saline. The ratio of RV/(LV + S) gradually increased from day 14 onwards. The open bars represent the data for the control rats ($n = 4$ for each bar), and solid bars represent the data for the MCT-treated rats ($n = 9$ for each bar). $^{*}P < 0.05$, $^{**}P < 0.01$ vs. control.

Downloaded from https://academic.oup.com/abbs/article/47/3/156/1754516 by guest on 05 April 2024

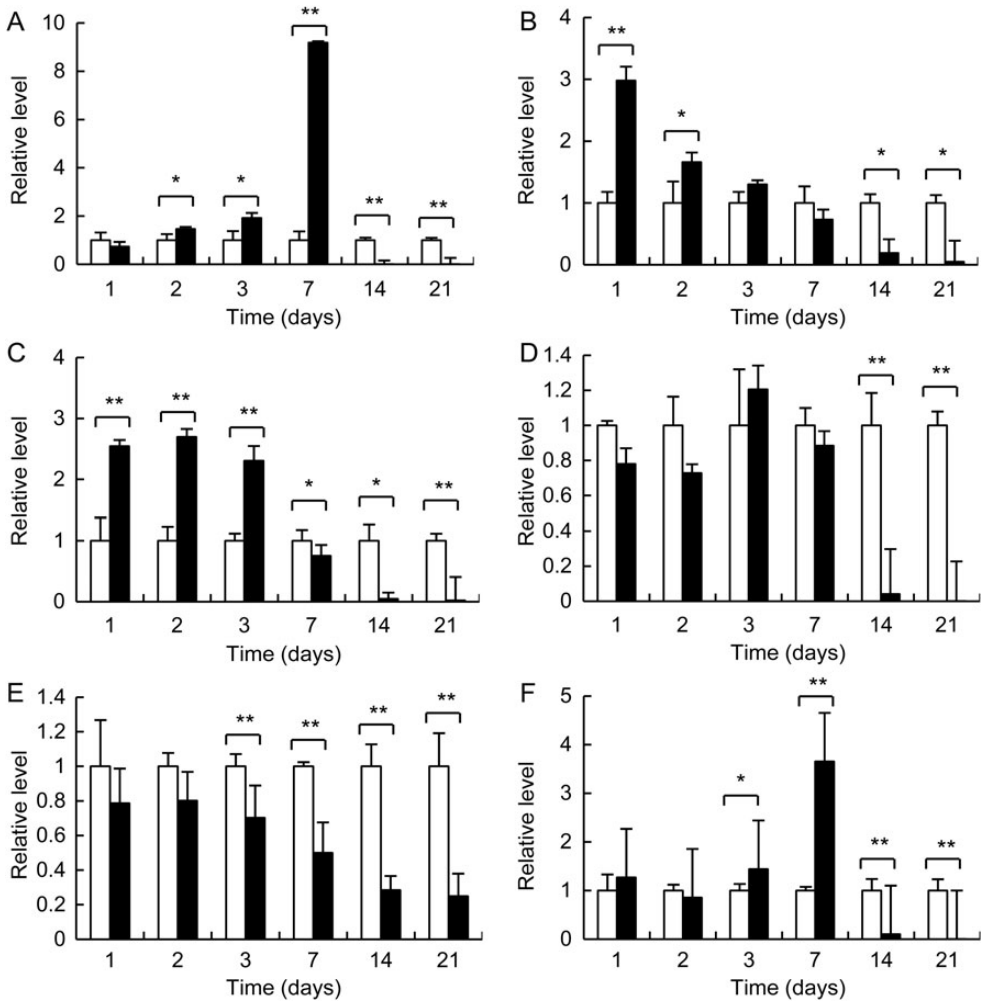

Figure 4. Effect of MCT on the mRNA expression of intracellular vesicular transport proteins and plasma membrane proteins Levels of mRNA expression for NSF (A), α-SNAP (B), synaptosome-associated membrane protein 23 (SNAP23) (C), BMPR2 (D), cav-1 (E), and eNOS (F) were analyzed by semiquantitative real-time PCR. Rats were sacrificed on days 1, 2, 3, 7, 14, and 21 after treatment with MCT. Rats treated with normal saline were used as controls. The data are results from three independent experiments. Open bars represent the data from the control rats, and solid bars represent the data from the MCT-treated rats. The normalized expression level of control group is set as '1'. $^{*}P < 0.05$, $^{**}P < 0.01$ vs. control.

7 (0.75, $P = 0.047$), and was barely detectable on days 14 and 21 ($P < 0.01$). The level of BMPR2 mRNA expression did not change significantly during days 1–7 (0.73–1.2, $P > 0.05$) and then significantly decreased from day 14 to day 21 ($P < 0.01$). After the first 2 days, the level of cav-1 mRNA expression in MCT-treated rats gradually decreased, and reached 25% of the level in control rats by day 21 ($P < 0.01$). The level of eNOS mRNA expression was elevated on days 3–7 (1.4 to 3.7 folds greater than that in control rats; $P < 0.05$), but started to decline on day 14 and was barely detectable on day 21 ($P < 0.01$).

Effect of MCT on protein expressions of NSF, α-SNAP, SNAP23, BMPR2, cav-1, and eNOS

A 76 kDa band for NSF, a 38 kDa band for α-SNAP, a 23 kDa band for SNAP23, a 130 kDa band for BMPR2, a 22 kDa band for cav-1, and a 140 kDa band for eNOS in rat lung tissue were identified by western blot analysis (**Fig. 5**). In MCT-treated rats, NSF protein expression increased on days 1–3 (1.2 to 2.3 folds greater than that in control rats; $P < 0.05$) but then significantly decreased from day 7 (0.65, $P = 0.004$) and was barely detectable after day 14 ($P < 0.001$). From day 1 to day 7, the level of α-SNAP protein expression in MCT-treated rats was 1.2 to 2.2 folds higher than that in control rats ($P < 0.01$) but then significantly decreased from day 14 onwards ($P < 0.05$). For the first 7 days after injection, the level of SNAP23 protein expression in MCT-treated rats was significantly higher than that in control rats (3 to 36 folds higher, $P < 0.05$) but then decreased to control level on day 14 ($P = 0.76$) and was significantly reduced by day 21 ($P = 0.028$). On days 1–3, the level of BMPR2 protein expression in MCT-treated rats was up-regulated by 1.7 to 2.3 folds compared with that in control rats ($P < 0.01$), but returned to control level on day 7 ($P = 0.41$) and was significantly reduced ($P < 0.01$) thereafter. The level of cav-1 protein expression in MCT-treated rats was down-regulated from day 7 (0.6 to 0.88 fold lower than that in control rats; $P < 0.01$). From day 1 to day 7, the level of eNOS protein expression in MCT-treated rats was 1.2 to 1.6 folds higher than that in control rats ($P < 0.05$), except on the day 3, when it was only 0.98 fold higher ($P = 0.38$); it was then reduced to 50%–67% of the control level from day 14 ($P < 0.01$).

Downloaded from https://academic.oup.com/abbs/article/47/3/156/1754516 by guest on 05 April 2024

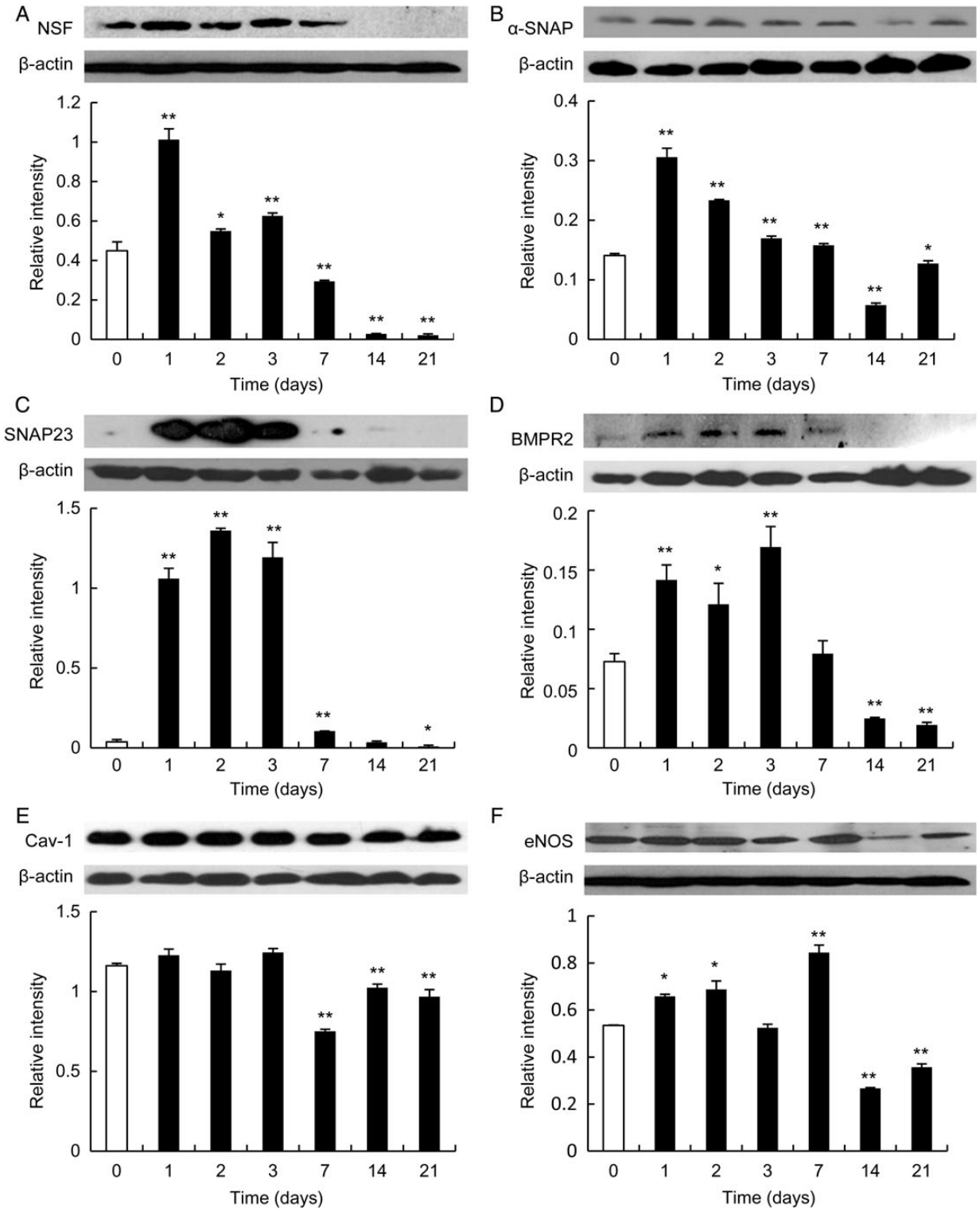

Figure 5. Effect of MCT on the protein expression of intracellular vesicular transport proteins and plasma membrane proteins Levels of protein expression for NSF (A), α-SNAP (B), SNAP23 (C), BMPR2 (D), cav-1 (E), and eNOS (F) were analyzed by western blot analysis. Rats were sacrificed on days 1, 2, 3, 7, 14, and 21 after treatment with MCT. Rats treated with normal saline were used as controls. The data are results from three independent experiments. Open bars represent data for the control rats, and solid bars represent data for the MCT-treated rats. $^{*}P<0.05$, $^{**}P<0.01$ vs. control.

Effects of MCT on caspase-3 activation

Abnormal apoptosis plays an important role in the pathogenesis of PAH. In order to analyze the relationship between the expression of vesicular transport proteins and apoptosis, the expression of caspase-3, an important effector enzyme for apoptosis was investigated by western blot analysis. The 20- and 17-kDa bands representing

Downloaded from https://academic.oup.com/abbs/article/47/3/156/1754516 by guest on 05 April 2024

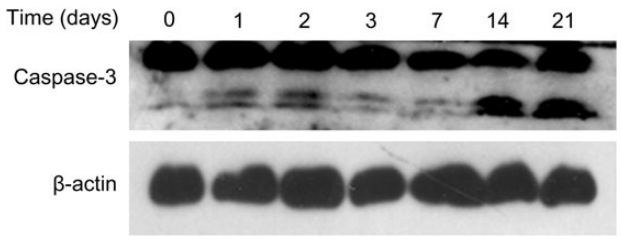

Figure 6. The effect of MCT on apoptosis Apoptosis was evaluated by examining caspase-3 expression via western blotting. Rats were sacrificed on days 1, 2, 3, 7, 14, and 21 after treatment with MCT. Rats treated with normal saline were used as controls. The 20- and 17-kDa bands represent the active forms of caspase-3 and the 32-kDa band represents the inactive form of caspase-3. The active forms of caspase-3 were increased after exposure to MCT, especially on days 14 and 21.

the active forms of caspase-3 and the 32-kDa band for the inactive form of caspase-3 were expressed in rat lungs (**Fig. 6**). It was found that the expression of the active forms of caspase-3 was increased in MCT-treated rats, especially on days 14 and 21.

Discussion

The transport of proteins to the target subcellular compartments and organelles is mediated by intracellular vesicular transport and subsequent membrane fusion, which involves tether proteins, NSF, SNAPs, and SNAREs [24–26]. The process is complicated. Briefly, tether proteins bring cargo vesicle and target membranes together; then, the vesicle and target membranes are fused following the formation of a complex by the SNARE proteins located on both membranes. Subsequently, SNAP protein (usually α-SNAP) recruits NSF to disassemble the complex for the next transportation [27–29]. Dysfunctional vesicular transport is an underlying cause for several diseases, such as Parkinson's disease, Alzheimer's disease, and lysosomal storage diseases [24,30,31]. Recent studies have shown that dysfunctional vesicular transport is a prelude to the development of PAH [16–23]. In experimentally induced PAH, diverse tethers, SNAREs, and SNAPs were found to be trapped in the Golgi, together with BMPR2, cav-1, and eNOS, while NSF was found to be largely sequestered in an intracellular location separate from the Golgi. These observations suggested that dysfunction occurred in the disassembly step in vesicular transport in PAH [17,18]. However, the expression patterns of vesicular transport proteins in PAH have not been reported. How do the expressions of vesicular transport proteins change as PAH progressively worsens? Are the changes in vesicular transport proteins accompanied by changes in the expression of plasma membrane proteins and in apoptosis? To address these questions, we examined the expressions of vesicular transport proteins NSF, α-SNAP, and SNAP23, the plasma membrane proteins BMPR2, cav-1, and eNOS, and the apoptosis marker caspase-3 in lung tissues from rats treated with either MCT or saline (control). It was found that, at both the mRNA and protein levels, NSF, α-SNAP, and SNAP23 were up-regulated prior to the appearance of PAH and down-regulated when the pulmonary arterial pressure increased, and that similar changes occurred in the expressions of BMPR2 and eNOS, although cav-1 was down-regulated only. Apoptosis, as indicated by caspase-3 protein expression, was also increased after exposure to MCT, and was greatly increased when PAH was established.

NSF is an ATPase required for the disassembly of all SNARE complexes. It can be covalently modified by NO-mediated *S*-nitrosylation, which makes it unable to disassemble SNARE complexes [32]. The protein α-SNAP is essential for the recruitment of NSF to SNARE complex [28,29,32]. SNAP23 forms clusters with syntaxin-4 in the plasma membrane, and these clusters serve as the fusion sites for caveolae during exocytosis [33]. They are very important in the intracellular vesicular transport. In this study, it was found that NSF, α-SNAP, and SNAP23 were uniformly up-regulated from the first day after administration of MCT, at a time largely preceding the development of PAH, and were then down-regulated from day 7 or day 14, as pulmonary arterial pressure increased. These data suggested that such changes in expression might not simply be a consequence of increased pulmonary arterial pressure, but instead, might function in the pathogenesis of PAH. However, the effect of up-regulated NSF, α-SNAP, and SNAP23 is not clear. In pulmonary arterial endothelial cells treated with MCT pyrrole and NO scavenger, exogenous secretion was markedly increased from day 2 of the assay and was sustained for the duration of the 5-day assay [16,18]. As inward transcription-targeted signaling involving the Smad-family and STAT3 transcription factors is associated with endocytic/caveolar vesicular transport, which itself involves NSF, SNAREs, SNAPs, and so on [34–39]. The down-regulation of NSF, α-SNAP, and SNAP23 may lead to dysfunctional Smad and STAT3 signaling, which is known to contribute to the development of PAH. Consistent with this, it was found that the levels of apoptosis were significantly increased when NSF, α-SNAP, and SNAP23 were down-regulated and pulmonary arterial pressure increased. Thus, this relationship merits further investigation. We hypothesize that there might be feedback mechanisms playing a role in the damage to vesicular transport caused by MCT: at first NSF, α-SNAP, and SNAP23 are up-regulated to maintain vesicular transport (negative feedback); however, decompensation causes their expressions to be down-regulated, which further aggravates the damaged vesicular transport and the disruption of the signaling pathway, leading to abnormal cellular growth and elevated pulmonary arterial pressure in a self-reinforcing manner (positive feedback).

BMPR2, cav-1, and eNOS are plasma membrane proteins that play an important role in PAH. BMP, a member of the transforming growth factor-β family, binds to BMPR2, and activates Smad-family transcription factors to inhibit cellular proliferation. Mutations in BMPR2 account for approximately one-half of the causes of familial PAH and one-quarter of the sporadic cased of PAH. Several versions of mutant BMPR2 fail to be trafficked correctly to the plasma membrane and are abnormally sequestered in the endoplasmic reticulum and the Golgi, while other versions able to be trafficked to the plasma membrane exhibit defective signaling [40–42]. It has been reported that there are reduced levels of BMPR2 and reduced BMP/Smad signaling, even when there are no mutations in BMPR2 in primary pulmonary hypertension [43]. Smad signaling is dependent on membrane-associated endocytic pathways [34]. Defects in intracellular vesicular transport might explain the defects in BMP/Smad signaling seen in idiopathic PAH in the absence of mutations in BMPR2. In our study, it was found that BMPR2 was significantly up-regulated during the first 3 days after MCT treatment, but only at the protein levels. This observation indicated that the up-regulation of BMPR2 occurred at the posttranslational level. Subsequently, BMPR2 was down-regulated at both the mRNA and protein levels from day 14 onwards.

Caveolae are 50–100 nm invaginations of the plasma membrane and are rich in cholesterol and sphingolipids. Caveolins are the structural proteins essential for the formation of caveolae in lipid raft domains. cav-1 is highly expressed in endothelial cells, adipocytes, and smooth muscle cells. It was found that cav-1 expression was reduced in the cells in plexiform lesions in patients with PAH [20,44] and in

Downloaded from https://academic.oup.com/abbs/article/47/3/156/1754516 by guest on 05 April 2024

rats treated with MCT [19], and *cav-1*$^{-/-}$ mice spontaneously developed PAH and dilated cardiomyopathy [45,46]. Loss of cav-1 from cell surface is inversely correlated with hyperactivation of promitogenic and antiapoptotic PY-STAT3 and ERK1/2 signaling, with DNA synthesis, and with the development of PAH [19,45,46]. BMPR2 is located in lipid rafts, including caveolae [47], and cav-1 can regulate the caveolar localization and transcriptional activation function of BMPR2 [48]. Reduction in cav-1 or the presence of a dominant-negative cav-1 can reduce BMPR2 plasma membrane localization and BMP-dependent Smad phosphorylation and gene regulation [48]. In this study, it was found that cav-1 was down-regulated in MCT-treated rats and this down-regulation might promote the formation of PAH through activating the PY-STAT3 and ERK1/2 signaling pathway and decreasing the BMP-Smad signaling.

NO levels are reduced in the pulmonary arterial walls in human and experimental PAH. However, eNOS levels have been reported to be unchanged, decreased, or even increased in PAH [17,49,50]. In this study, the expression of eNOS was found to be first up-regulated in response to MCT and then down-regulated after pulmonary arterial pressure started to increase. Extracellular NO is derived from cell surface caveolar eNOS. However, MCT treatment causes eNOS to be lost from cell surface caveolae and be trapped in the intracellular compartments, such as Golgi and endoplasmic reticulum [17,51]. Although NO can still be generated by eNOS, it cannot reach the extracellular space. Consequently, the amount of NO in the pulmonary arterial vasculature is reduced [17]. The intracellular NO causes S-nitrosylation of NSF and thus further inhibits vesicular transport in a self-reinforcing inhibitory loop [52]. Based on these findings, we speculate that increased levels of eNOS may inhibit NSF, leading to an exacerbation of dysfunctional vesicular transport, and that decreased eNOS levels may lead to a shortage of NO and thus promote the elevation of pulmonary arterial pressure.

One limitation of our study is that the whole lung was examined, not the pulmonary vasculature. Indeed, it has been shown that the cellular targets of MCT include the pulmonary arterial endothelial cell, pulmonary arterial smooth muscle cell, and alveolar epithelial cell [22,23]. In future studies, immunofluorescence and *in situ* hybridization study will be used to determine whether vascular cells also exhibit changes in the expression of intracellular vesicular transport proteins in response to MCT.

In summary, we found that in MCT-treated rats, the expressions of NSF, α-SNAP, and SNAP23 were up-regulated at both mRNA and protein levels prior to the formation of PAH and down-regulated after the establishment of PAH. These expression changes were accompanied by abnormal expressions of BMPR2, cav-1, and eNOS, and by increased levels of apoptosis as well. Nevertheless, NSF, α-SNAP, and SNAP23 appear to be mechanistically associated with the development of PAH in MCT-treated rats. Thus, the possible roles of these proteins in the pathogenesis of PAH merit further study.

Acknowledgments

We would like to thank Dr James E. Hansen at Respiratory and Critical Care Physiology and Medicine, Harbor-UCLA Medical Center, Los Angeles Biomedical Research and Education Institute, St John's Cardiovascular Research Center, California, USA for his help in language editing.

Funding

This work was supported by a grant from the National Natural Science Foundation of China (No. 30871056).

References

1. McLaughlin VV, Archer SL, Badesch DB, Barst RJ, Farber HW, Lindner JR, Mathier MA, *et al*. ACCF/AHA 2009 expert consensus document on pulmonary hypertension a report of the American College of Cardiology Foundation Task Force on Expert Consensus Documents and the American Heart Association developed in collaboration with the American College of Chest Physicians; American Thoracic Society, Inc.; and the Pulmonary Hypertension Association. *J Am Coll Cardiol* 2009, 53: 1573–1619.
2. Higenbottam T, Naeije R, Voelkel NF, Botney MD, Christman B, Giald A, Hales CA, *et al*. Pathobiology of pulmonary hypertension. In: Rich S, editor. *Primary Pulmonary Hypertension: Executive Summary from the World Symposium on Primary Pulmonary Hypertension 1998*. Available from the World Health Organization at http://www.who.int/ncd/cvd/pph.html.
3. Humbert M, Morrell NW, Archer SL, Stenmark KR, MacLean MR, Lang IM, Christman BW, *et al*. Cellular and molecular pathobiology of pulmonary arterial hypertension. *J Am Coll Cardiol* 2004, 43: 13S–24S.
4. Cool CD, Groshong SD, Oakey J, Voelkel NF. Pulmonary hypertension cellular and molecular mechanisms. *Chest* 2005, 128: 565S–571S.
5. D'Alonzo GE, Barst RJ, Ayres SM, Bergofsky EH, Brundage BH, Detre KM, Fishman AP, *et al*. Survival in patients with primary pulmonary hypertension: results from a national prospective registry. *Ann Intern Med* 1991, 115: 343–349.
6. Benza RL, Miller DP, Barst RJ, Badesch DB, Frost AE, McGoon MD. An evaluation of long-term survival from time of diagnosis in pulmonary arterial hypertension from the REVEAL Registry. *Chest* 2012, 142: 448–456.
7. Heath D, Smith P, Gosney J, Mulcahy D, Fox K, Yacoub M, Harris P. The pathology of early and late stages of primary pulmonary hypertension. *Br Heart J* 1987, 58: 204–213.
8. Smith P, Heath D. Electron microscopy of the plexiform lesion. *Thorax* 1979, 34: 177–186.
9. Smith P, Heath D, Yacoub M, Madden B, Caslin A, Gosney J. The ultrastructure of plexogenic pulmonary arteriopathy. *J Pathol* 1990, 160: 111–121.
10. Merkow L, Kleinerman J. An electron microscopic study of pulmonary vasculitis induced by monocrotaline. *Lab Invest* 1966, 15: 547–564.
11. Rosenberg HC, Rabinovitch M. Endothelial injury and vascular reactivity in monocrotaline pulmonary hypertension. *Am J Physiol Heart Circ Physiol* 1988, 255: H484–H491.
12. Meyrick B, Reid L. Hypoxia-induced structural changes in the media and adventitia of the rat hilar pulmonary artery and their regression. *Am J Pathol* 1980, 100: 151–178.
13. Jaenke RS, Alexander AF. Fine structural alterations of bovine peripheral pulmonary arteries in hypoxia-induced hypertension. *Am J Pathol* 1973, 73: 377–398.
14. King AP, Smith P, Heath D. Ultrastructure of rat pulmonary arterioles after neonatal exposure to hypoxia and subsequent relief and treatment with monocrotaline. *J Pathol* 1995, 177: 71–81.
15. Reindel JF, Roth RA. The effects of monocrotaline pyrrole on cultured bovine pulmonary artery endothelial and smooth muscle cells. *Am J Pathol* 1991, 138: 707–719.
16. Lee J, Reich R, Xu F, Sehgal PB. Golgi, trafficking, and mitosis dysfunctions in pulmonary arterial endothelial cells exposed to monocrotaline pyrrole and NO scavenging. *Am J Physiol Lung Cell Mol Physiol* 2009, 297: L715–L728.
17. Mukhopadhyay S, Xu F, Sehgal PB. Aberrant cytoplasmic sequestration of eNOS in endothelial cells after monocrotaline, hypoxia and senescence: subcellular eNOS localization and live-cell caveolar and cytoplasmic NO imaging studies. *Am J Physiol Heart and Circ Physiol* 2007, 292: H1373–H1389.
18. Sehgal PB, Mukhopadhyay S, Xu F, Patel K, Shah M. Dysfunction of Golgi tethers, SNAREs and SNAPs in monocrotaline-induced pulmonary hypertension. *Am J Physiol Lung Cell Mol Physiol* 2007, 292: L1526–L1542.
19. Mathew R, Huang J, Shah M, Patel K, Gewitz M, Sehgal PB. Disruption of endothelial cell caveolin-1alpha/raft scaffolding during development of monocrotaline-induced pulmonary hypertension. *Circulation* 2004, 110: 1499–1506.

Downloaded from https://academic.oup.com/abbs/article/47/3/156/1754516 by guest on 05 April 2024

20. Achcar RO, Demura Y, Rai PR, Taraseviciene-Stewart L, Kasper M, Voelkel NF, Cool CD. Loss of caveolin and heme oxygenase expression in severe pulmonary hypertension. *Chest* 2006, 129: 696–705.
21. Shah M, Patel K, Sehgal PB. Monocrotaline induced endothelial cell megalocytosis involves a Golgi blockade mechanism. *Am J Physiol Cell Physiol* 2005, 288: C850–C862.
22. Mukhopadhyay S, Sehgal PB. Discordant regulatory changes in monocrotaline induced megalocytosis of lung arterial endothelial and alveolar epithelial cells. *Am J Physiol Lung Cell Mol Physiol* 2006, 290: L1216–L1226.
23. Mukhopadhyay S, Shah M, Patel K, Sehgal PB. Monocrotaline pyrrole-induced megalocytosis of lung and breast epithelial cells: disruption of plasma membrane and Golgi dynamics and an enhanced unfolded protein response. *Toxicol Appl Pharmacol* 2006, 211: 209–220.
24. Cooper AA, Gitler AD, Cashika A, Haynes CM, Hill KJ, Bhullar B, Liu K, *et al*. Alpha-synuclein blocks ER-Golgi traffic and Rab1 rescues neuron loss in Parkinson's models. *Science* 2006, 313: 324–328.
25. Fries E, Rothman JE. Transport of vesicular stomatitis virus glycoprotein in a cell-free extract. *Proc Natl Acad Sci USA* 1980, 77: 3870–3874.
26. Gissen P, Johnson CA, Morgan NV, Stapelbroek JM, Forshew T, Cooper WN, McKiernan PJ, *et al*. Mutations in VPS33B, encoding a regulator of SNARE dependent membrane fusion, cause arthrogryposis-renal dysfunction-cholestasis (ARC) syndrome. *Nat Genet* 2004, 36: 400–404.
27. Stow JL, Manderson AP, Murray RZ. SNAREing immunity: the role of SNAREs in the immune system. *Nat Rev Immunol* 2006, 6: 919–929.
28. Jahn R, Scheller RH. SNAREs-engines for membrane fusion. *Nat Rev Mol Cell Biol* 2006, 7: 631–643.
29. Bonifacino JS, Glick BS. The mechanism of vesicle budding and fusion. *Cell* 2004, 116: 153–166.
30. Suzuki T, Araki Y, Yamamoto T, Nakaya T. Trafficking of Alzheimer's disease-related membrane proteins and its participation in disease pathogenesis. *J Biochem* 2006, 139: 949–955.
31. Hopkin RJ, Grabowski GA. Lysosomal storage diseases. In: Kasper DL, Braunwald E, Fauci AS, Hauser SL, Longo DL, Jameson JL eds. *Harrison's Principles of Internal Medicine*. 16th edn. New York: McGraw-Hill, 2005, 2315–2319.
32. Matsushita K, Morrell CN, Cambien B, Yang SX, Yamakuchi M, Bao C, Hara MR, *et al*. Nitric oxide regulates exocytosis by S-nitrosylation of N-ethlymaleimide sensitive factor. *Cell* 2003, 115: 139–150.
33. Predescu SA, Predescu DN, Shimizu K, Klein IK, Malik AB. Cholesterol-dependent syntaxin-4 and SNAP-23 clustering regulates caveolar fusion with the endothelial plasma membrane. *J Biol Chem* 2005, 280: 37130–37138.
34. Di Guglielmo GM, Le Roy C, Goodfellow AF, Wrana JL. Distinct endocytic pathways regulate TGF-beta receptor signaling and turnover. *Nat Cell Biol* 2003, 5: 410–421.
35. Sehgal PB, Guo GG, Shah M, Kumar V, Patel K. Cytokine signaling: STATs in plasma membrane rafts. *J Biol Chem* 2002, 277: 12067–12074.
36. Shah M, Patel K, Mukhopadhyay S, Xu F, Guo G, Sehgal PB. Membrane-associated STAT3 and PY-STAT3 in the cytoplasm. *J Biol Chem* 2006, 281: 7302–7308.
37. Xu F, Mukhopadhyay S, Sehgal PB. Live cell imaging of interleukin-6-induced targeting of the "transcription factor" STAT3 to sequestering endosomes in the cytoplasm. *Am J Physiol Cell Physiol* 2007, 293: C1374–C1382.
38. Mukhopadhyay S, Shah M, Xu F, Patel K, Tuder RM, Sehgal PB. Cytoplasmic provenance of STAT3 and PY-STAT3 in the endolysosomal compartments in pulmonary arterial endothelial and smooth muscle cells: implication in pulmonary arterial hypertension. *Am J Physiol Lung Cell Mol Physiol* 2007, 294: L449–L468.
39. Le Borgne R. Regulation of Notch signaling by endocytosis and endosomal sorting. *Curr Opin Cell Biol* 2006, 18: 213–222.
40. Morrell NW. Role of bone morphogenetic protein receptors in the development of pulmonary hypertension. *Adv Exp Med Biol* 2010, 661: 251–264.
41. Nishihara A, Watabe T, Imamura T, Miyazono K. Functional heterogeneity of bone morphogenetic protein receptor-II mutants found in patients with primary pulmonary hypertension. *Mol Biol Cell* 2002, 13: 3055–3063.
42. Rudarakanchana N, Flanagan JA, Chen H, Upton PD, Machado R, Patel D, Trembath RC, *et al*. Functional analysis of bone morphogenetic protein type II receptor mutations underlying primary pulmonary hypertension. *Hum Mol Genet* 2002, 11: 1517–1525.
43. Atkinson C, Stewart S, Upton PD, Machado R, Thomson JR, Trembath RC, Morrell NW. Primary pulmonary hypertension is associated with reduced pulmonary vascular expression of type II bone morphogenetic protein receptor. *Circulation* 2002, 105: 1672–1678.
44. Jasmin JF, Mercier I, Hnasko R, Cheung MW, Tanowitz HB, Dupuis J, Lisanti MP. Lung remodeling and pulmonary hypertension after myocardial infarction: pathogenic role of reduced caveolin expression. *Cardiovasc Res* 2004, 63: 747–755.
45. Zhao YY, Lui Y, Stan RV, Fan L, Gu Y, Dalton N, Chu PH, *et al*. Defects in caveolin-1 cause dilated cardiomyopathy and pulmonary hypertension in knockout mice. *Proc Natl Acad Sci USA* 2002, 99: 11375–11380.
46. Zhao YY, Zhao YD, Mirza MK, Huang JH, Potula HH, Vogel SM, Brovkovych V, *et al*. Persistent eNOS activation secondary to caveolin-1 deficiency induces pulmonary hypertension in mice and humans through PKG nitration. *J Clin Invest* 2009, 119: 2009–2018.
47. Ramos M, Lame MW, Segall HJ, Wilson DW. The BMP type II receptor is located in lipid rafts, including caveolae, of pulmonary endothelium *in vivo* and *in vitro*. *Vasc Pharmacol* 2006, 44: 50–59.
48. Wertz JW, Bauer PM. Caveolin-1 regulates BMPR II localization and signaling in vascular smooth muscle cells. *Biochem Biophys Res Commun* 2008, 375: 557–561.
49. Giaid A, Saleh D. Reduced expression of endothelial nitric oxide synthase in lungs of patients with pulmonary hypertension. *N Engl J Med* 1995, 333: 214–221.
50. Tyler RC, Muramatsu M, Abman SH, Stelzer TJ, Rodman DM, Bloch KD, McMurtry IF. Variable expression of endothelial NO synthase in three forms of rat pulmonary hypertension. *Am J Physiol* 1999, 276: L297–L303.
51. Murata T, Sato K, Hori M, Ozaki H, Karaki H. Decreased endothelial nitric-oxide synthase (eNOS) activity resulting from abnormal interaction between eNOS and its regulatory proteins in hypoxia-induced pulmonary hypertension. *J Biol Chem* 2002, 277: 44085–44092.
52. Iwakiri Y, Satoh A, Chatterjee S, Toomre DK, Chalouni CM, Fulton D, Grozmann RJ, *et al*. Nitric oxide synthase generates nitric oxide locally to regulate compartmentalized protein S-nitrosylation and protein trafficking. *Proc Natl Acad Sci USA* 2006, 103: 19777–19782.

Downloaded from https://academic.oup.com/abbs/article/47/3/156/1754516 by guest on 05 April 2024